

Melting Characteristics of C-Type Filler Metal in GTAW

A C-type filler metal's effect on deposition rate, penetration depth, and metal transfer is analyzed

BY M. CHEEPU, H. J. BAEK, Y. S. KIM, AND S. M. CHO

Abstract

A C-type filler metal was developed to overcome the low deposition rate (DR) of gas tungsten arc welding (GTAW). The present study investigated the maximum DR for a novel C-type filler metal and compared it to conventional circular welding wires during GTAW using an Alloy 625 filler metal. For comparison with conventional circular welding wires, a $\varnothing 1.2$ -mm (0.047-in.) welding wire, which is most widely used in practice, and a $\varnothing 2.4$ -mm (0.094-in.) welding wire, which has almost the same sectional area as the novel C-type filler metal, were used in this research. An industrial robot was utilized to produce bead-on-plate welds in the flat position. The results revealed that at the same 200-A welding current, the DR of the C-type filler metal was higher than the conventional circular welding wires by 1.17 to 1.4 times according to the sectional area of the circular welding wires. At a high welding current of 500 A, it was impossible for the $\varnothing 1.2$ -mm welding wire to deposit quality welds, and the acceptable range of the DR for the $\varnothing 2.4$ -mm welding wire was narrow (i.e., 7–8 kg/h [15.4–17.6 lb/h]). However, the acceptable range of the DR for the C-type filler metal was as broad as 5.04–12.1 kg/h (11.1–26.6 lb/h) under the high welding current of 500 A. The maximum DR of the C-type filler metal was 1.51 times that of the $\varnothing 2.4$ -mm welding wire. The mechanism of obtaining a high DR using the C-type filler metal was analyzed from the viewpoint of the continuous bridging transfer at the melting edge of the C-type filler metal. The ability of the C-type filler metal to achieve high DRs at high-current regions was superior to the conventional $\varnothing 1.2$ - and $\varnothing 2.4$ -mm welding wires.

Keywords

- Gas Tungsten Arc Welding (GTAW)
- Filler Metal
- C-Type Filler Metal
- Welding Wire
- Deposition Rate (DR)
- Fusion Depth/Penetration Depth
- Metal Transfer
- Continuous Bridging Transfer
- Welding Current
- Filler Metal Current

Introduction

Excellent welding quality can be obtained via automatic gas tungsten arc welding (GTAW) with a filler metal if continuous bridging transfer is implemented. However, the productivity of automatic GTAW with a conventional circular welding wire is low. Therefore, many technologies have been developed to increase the deposition rate (DR) of GTAW (Ref. 1). A higher DR requires a higher welding current and speed. However, humping beads may appear in the high-current region of GTAW (Ref. 2).

Therefore, a C-type filler metal was developed as the filler metal of GTAW to increase the DR in the high-current region (Ref. 3). The wide and unique shape of the C-type filler metal could prevent high arc pressure on the weld pool when used in high-current GTAW. Additionally, a high DR could be obtained even though a cold filler metal was used (Refs. 4–6). Hence, GTAW with a C-type filler metal is more effective for weld overlay and wire arc additive manufacturing (WAAM) (Refs. 7, 8). Obtaining a small and stable fusion depth is important in the overlay and WAAM. For the purpose of this paper, fusion depth shall be referred to as penetration depth. This penetration depth may be affected by metal transfer from the melting edge of the filler metal to the weld pool (Ref. 9). However, before this research, a direct comparison between C-type filler metals and circular welding wires in terms of metal transfer and penetration depth had not been performed.

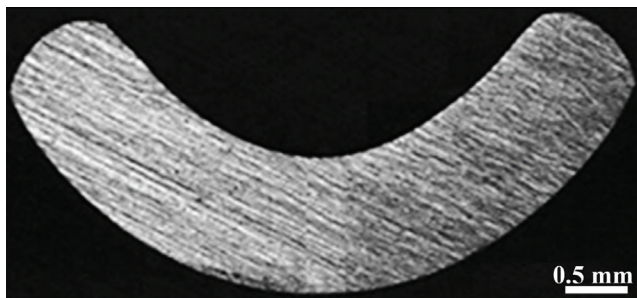


Fig. 1 – Cross-sectional area of a newly developed C-type filler metal.

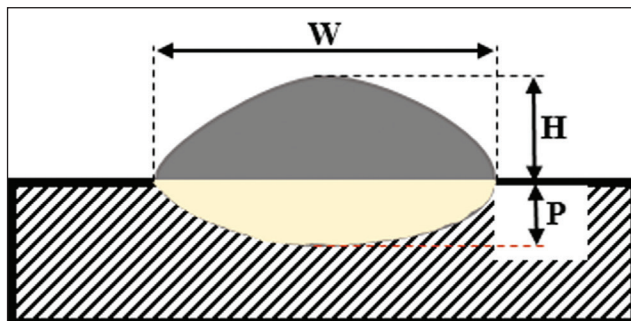


Fig. 2 – Definition and measurement of the bead geometry. Note: penetration depth = P , bead width = W , and reinforcement height = H .

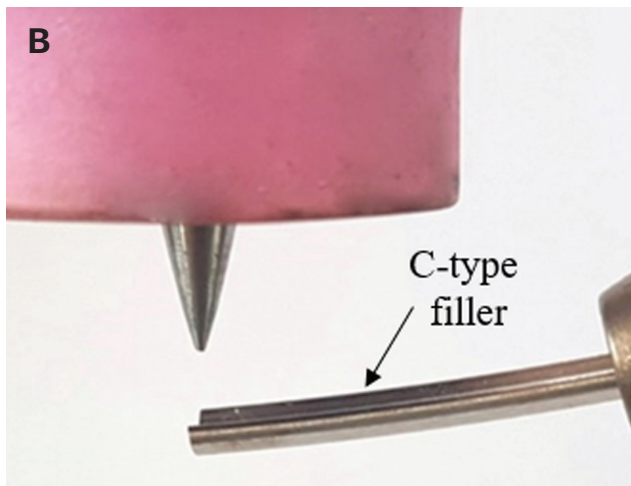
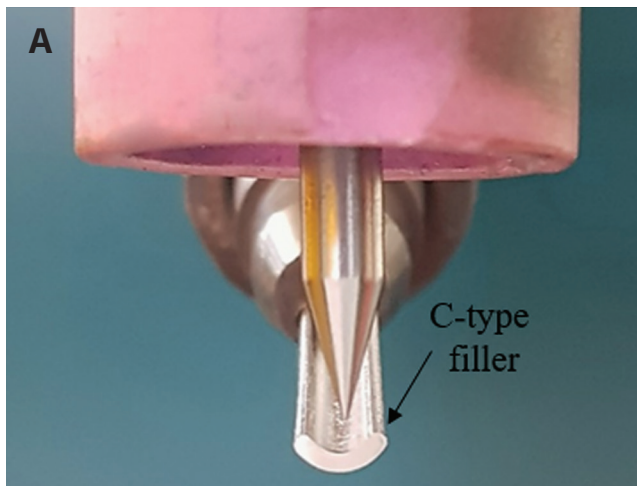


Fig. 3 – Schematic of GTAW with a C-type filler metal: A – Front view; B – side view.

In general, arc radiation may partially melt the filler metal during GTAW, but the plasma stream of the arc can melt it primarily. We considered the plasma stream to obtain a high DR of the C-type filler metal (Refs. 6, 7, 10).

This study aimed to establish a model for metal transfer and penetration depth using GTAW at a current of 200 and 500 A with C-type filler metals and conventional welding wires. In addition, the maximum DRs at each welding current were investigated for the C-type filler metals and circular welding wires. The melting edge and bridge of the filler metal in the arc were observed using a welding camera.

Experimental Procedure

An ASTM A283 plate ($t = 10$ mm [0.39 in.]) was used as a substrate for the bead-on plate welds using GTAW with Alloy 625 (ERNiCrMo-3) filler metal. Three types of filler metals/welding wires were used in the experiments. These were a $\phi 1.2$ -mm (0.047-in.) welding wire (usually used in automatic GTAW), a $\phi 2.4$ -mm (0.094-in.) welding wire (the cross-sectional area is the same as a C-type filler metal), and a newly developed C-type filler metal of 5 mm² (width: 5 mm [0.196 in.]; thickness: 1 mm [0.039 in.]) – Fig. 1.

A tungsten electrode (W-electrode) with a diameter of 4 mm (0.157 in.) was used. The conical angle was 30 deg and the truncated tip size was 0.5 mm (0.019 in.) for 200 A. The

conical angle was 40 deg and the truncated tip size was 1.5 mm (0.059 in.) for 500 A. A mixed gas of Ar + 7% H_2 was used as the shielding gas at a flow rate of 20 L/min (5 gal/min). The stand-off distance between the electrode and the base metal was 5 mm, which was kept before welding. Before arc starting, the filler metal height between the filler tip bottom and the substrate surface was set to 0 mm, and the filler metal distance between the filler tip and the electrode center was set to 0 mm. The experiments were conducted using the standard procedure described in ISO/TR 18491, *Welding and allied processes – Guidelines for measurement of welding energies* (Refs. 11–13). An industrial six-axis robot was used to produce the beads. The waveforms of the welding arc voltage were monitored using an arc monitoring system for GTAW. The in-situ observations on the metal transfer behavior of the three welding wires/filler metals in various conditions were captured using a welding camera at a frame rate of 50 fps. The welds were cross sectioned and polished for macrosection analysis. The penetration depth was measured using software after etching the cross sections.

Figure 2 shows the measured geometry of the welds: penetration depth, bead width, and reinforcement height. The deepest penetration depth of the bead was considered the penetration depth. The penetration depth was calculated by taking the average of the three cross sections. Penetration depths greater than 0.3 mm (0.011 in.) and less than 3.0 mm (0.118 in.) were considered. If the penetration depth is smaller

Table 1 – Welding Parameters Used with Different Welding Wires and Filler Metals at 200 A

Welding Conditions				Results			
Ø1.2-mm welding wire							
Welding current (A)	Welding speed (cm/min)	Filler metal feed speed (cm/min)	Deposition area (mm ²)	Deposition rate (kg/h)	Penetration depth (mm)	W/H	Remarks
200	20.0	200	11.0	1.10	1.68	4.22	Good
		250	13.8	1.39	1.25	3.35	Good
		300	16.5	1.67	1.01	2.67	Good
		350	19.3	1.94	0.93	2.19	Good
		400	22.0	2.21	0.81	1.89	Good
		450	24.8	2.49	0.71	1.53	Good
		488	26.8	2.70	–	–	Sticking
		540	29.7	2.99	–	–	Sticking
630	34.7	3.49	–	–	Sticking		
Ø2.4-mm welding wire							
200	20.0	44.0	9.94	1.00	1.29	5.28	Good
		66.0	14.9	1.50	0.82	3.69	Good
		88.0	19.9	2.00	0.70	3.14	Good
		110	24.9	2.50	0.62	2.75	Good
		132	29.8	3.00	0.57	2.28	Good
		154	34.8	3.50	–	–	Sticking
C-type filler metal							
200	20.0	40.0	10.0	1.00	1.17	5.46	Good
		60.0	15.0	1.51	0.74	4.01	Good
		80.0	20.0	2.01	0.62	3.21	Good
		100	25.0	2.52	0.52	2.68	Good
		120	30.0	3.02	0.47	2.32	Good
		140	35.0	3.52	0.41	1.99	Good
		160	40.0	4.03	–	–	Sticking

Table 1 – continued

Welding Conditions				Results			
C-type filler metal							
Welding current (A)	Welding speed (cm/min)	Filler metal feed speed (cm/min)	Deposition area (mm ²)	Deposition rate (kg/h)	Penetration depth (mm)	W/H	Remarks
200	40.0	40.0	5.00	1.00	1.33	5.29	Good
		60.0	7.50	1.51	0.89	3.95	Good
		80.0	10.0	2.01	0.63	3.13	Good
		100	12.5	2.52	0.58	2.63	Good
		120	15.0	3.02	0.51	2.26	Good
		140	17.5	3.52	0.42	1.74	Good
		160	20.0	4.03	—	—	Sticking

than 0.3 mm, welding defects such as insufficient penetration depth and lack of penetration depth may appear in any weld. If the penetration depth is larger than 3.0 mm, dilution increases in overlay welding and worsens the wall resolution in WAAM. The penetration depth data of the welds, which included tunnel defects, undercuts, and humping beads, were excluded. The process setup with the C-type filler metal is shown in Fig. 3.

The welding conditions used in the experiments are listed in the Welding Conditions section of Tables 1 and 2. The deposition area (DA) and DR were calculated using the cross-sectional area of the filler metal, filler metal feed speed, and welding speed, as given in Equations 1 and 2.

$$DA = (A_F \times FFS) / U \quad (1)$$

$$DR = (A_F \times FFS \times \rho_F) \times 3600/1000 \quad (2)$$

$$NHI = \eta_a \times (I \times E) / U \quad (3)$$

$$NHIR = NHI/DA = \eta_a \times (I \times E)/(A_F \times FFS) \quad (4)$$

where the DA of the bead cross section is in mm², A_F is the cross-sectional area of the filler metal (mm²), FFS is the filler

metal feed speed (mm/s), U is the welding speed (mm/s), the DR is measured in kg/h, ρ_F is the density of the filler metal (g/mm³ [the density of Alloy 625 is 0.0084 g/mm³]), NHI is the net heat input (J/mm), η_a is the arc efficiency, I is the welding current (A), E is the voltage (V), and NHIR is the net heat input ratio (J/mm³).

Results and Discussion

Bead Appearance and Macrosection of the Welds

Figure 4A shows the typical bead appearance of the welds made with a ø1.2-mm welding wire, ø2.4-mm welding wire, and C-type filler metal at a welding current of 200 A. The bead appearances were almost similar at a DR of 1 kg/h (2.2 lb/h) for the two welding wires in the presence of uniform bead ripples formed by intermittent bridging transfer. In the case of the C-type filler metal, the bead surface was smooth, owing to the continuous bridging transfer. However, when the DR was increased to 2.5 kg/h (5.5 lb/h), the ø1.2-mm welding wire showed signs of slight sticking, whereas the ø2.4-mm welding wire and C-type filler metal showed sound beads. Further increasing the DR resulted in more sticking at the DR of 2.7 kg/h (5.9 lb/h) for the ø1.2-mm welding wire. On the contrary, for the ø2.4-mm welding wire, sticking appeared at the DR of 3.5 kg/h (7.7 lb/h).

In this study, only sound beads without sticking were considered to determine the maximum DR. Sticking and humping beads were considered defects, as seen in Tables 1 and 2. DuPont and Marder (Ref. 14) investigated the maximum DR of GTAW and plasma arc welding. The maximum volumetric filler metal (ø1.2-mm welding wire) feeding speed limit was

Table 2 – Welding Parameters Used with Different Welding Wires and Filler Metals at 500 A

Welding Conditions				Results					
Ø1.2-mm welding wire									
Welding current (A)	Welding speed (cm/min)	Filler metal feed speed (cm/min)	Deposition area (mm ²)	Deposition rate (kg/h)	Penetration depth (mm)	W/H	Remarks		
500	20.0	900	49.5	5.00	–	–	Humping		
	40.0	900	24.8	5.00	–	–	Humping		
	60.0	900	16.5	5.00	–	–	Humping		
		1443	26.5	8.00	–	–	Unstable welding wire feeding		
		1623	30.0	9.00	–	–			
		2165	39.7	12.00	–	–			
Ø2.4-mm welding wire									
500	20.0	220	49.7	5.01	–	–	Humping		
	40.0	220	24.9	5.01	–	–	Humping		
	60.0	220	16.6	5.01	–	–	Humping		
		264	19.9	6.01	–	–	Humping		
		308	23.2	7.01	2.86	2.71	Good		
		352	26.5	8.01	2.53	2.47	Good		
		396	29.8	9.02	–	–	Sticking		
		440	33.1	10.02	–	–	Sticking		
		483	36.4	11.00	–	–	Sticking		
		527	39.7	12.01	–	–	Sticking		
		C-type filler metal							
		500	20.0	160	40.0	4.03	–	–	Humping
200	50.0			5.04	4.72	4.26	Good		
240	60.0			6.05	3.69	3.78	Good		
280	70.0			7.05	2.43	3.67	Good		
320	80.0			8.06	1.78	3.18	Good		
360	90.0			9.07	1.28	2.65	Good		

Table 2 – continued

Welding Conditions				Results			
C-type filler metal							
Welding current (A)	Welding speed (cm/min)	Filler metal feed speed (cm/min)	Deposition area (mm ²)	Deposition rate (kg/h)	Penetration depth (mm)	W/H	Remarks
500	20.0	400	100	10.0	1.09	2.38	Good
		440	110	11.0	0.87	2.25	Good
		480	120	12.1	0.61	1.84	Good
		520	130	13.1	—	—	Sticking
	40.0	160	20.0	4.03	—	—	Humping
		200	25.0	5.04	4.76	3.38	Good
		240	30.0	6.05	3.81	3.41	Good
		280	35.0	7.05	2.57	3.17	Good
		320	40.0	8.06	2.12	2.71	Good
		360	45.0	9.07	1.61	2.54	Good
		400	50.0	10.0	1.15	2.32	Good
		440	55.0	11.0	0.95	1.96	Good
		480	60.0	12.1	0.69	1.65	Good
		520	65.0	13.1	—	—	Sticking
	60.0	160	13.3	4.03	—	—	Humping
		200	16.7	5.04	3.06	2.75	Good
		240	20.0	6.05	2.93	2.11	Good
		280	23.3	7.05	2.64	2.40	Good
		320	26.7	8.06	2.24	2.23	Good
		360	30.0	9.07	1.49	1.98	Good
		400	33.3	10.0	1.16	1.80	Good
		440	36.7	11.0	0.90	1.59	Good
		480	40.0	12.1	0.71	1.45	Good
		520	43.3	13.1	—	—	Sticking

DR (kg/h)	ø1.2mm wire	ø2.4mm wire	C-type filler	A
1.00				
2.50				
3.00				
3.50	Sticking			
4.00	Sticking	Sticking		10mm

I = 200A, U = 20.0 cm/min

DR (kg/h)	ø1.2mm wire	ø2.4mm wire	C-type filler	B
5.00	Humping bead	Humping bead		
8.00				
9.00		Sticking		
12.0	Unstable wire feeding	Sticking		
13.0		Sticking	Sticking	10mm

Welding direction →

I = 500A, U = 60.0 cm/min

Fig. 4 – Typical bead appearances according to the DR.

130 mm³/s (3.5 kg/h), owing to its low thermal efficiency and far wire movement from the arc column by large lateral vibrations at 400 A. In contrast, in this study of the welding current at 200 A, the bead appearance of the C-type filler metal was sound at the same DR of 3.5 kg/h without any sticking. Furthermore, at the same 200-A current for the C-type filler metal, sticking occurred when the DR increased to 4 kg/h (8.8 lb/h).

Figure 4B shows the bead appearance at 500 A. The ø1.2- and ø2.4-mm welding wires formed humping beads at a DR of 5 kg/h (11 lb/h). Shirali et al. (Ref. 15) mentioned that the weld bead geometry changed according to the welding current and caused humping and undercut defects during GTAW without the addition of filler metal. In this study, humping also appeared in the beads with the addition of welding wires because the welding current was very high at 500 A. Meanwhile, the bead appearances of the C-type filler metal were sound without any imperfections at DRs ranging from 5.04

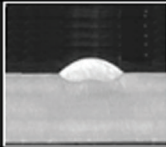
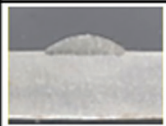
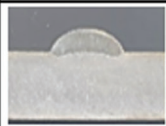
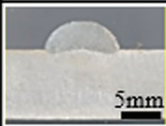
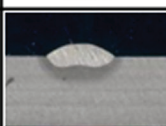
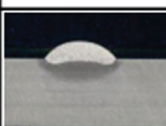
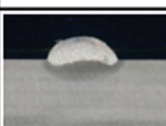
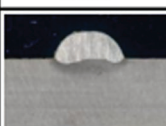
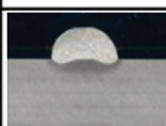
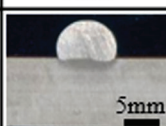
to 12.1 kg/h (11 to 26.6 lb/h). The sticking started to form at a DR of 13 kg/h (28.6 lb/h) for the C-type filler metal whereas the sticking occurred at a DR of 9 kg/h (19.8 lb/h) for the ø2.4-mm welding wire.

Figure 5 exhibits the macrosection of welds for the ø1.2-mm welding wire, ø2.4-mm welding wire, and C-type filler metal at currents of 200 and 500 A. The penetration depths were measured using macrosections. The penetration depths gradually decreased with the DR of all types of filler metals. Also, the reinforcement height gradually increased with the DR.

Effect of Process Parameters and Filler Metal Shape on Penetration Depth

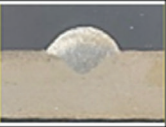
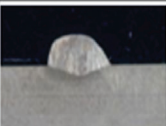
The results data on penetration depth and width/height (W/H) are listed in the Results section in Tables 1 and 2.

A

ø1.2mm wire							
DR(kg/h)	1.10	1.67	1.94	2.49	≥2.70		
Macro section					Sticking		
							
ø2.4mm wire							
DR(kg/h)	1.00	1.50	2.00	2.50	3.00	≥3.50	
Macro section						Sticking	
							
C-type filler							
DR(kg/h)	1.00	1.51	2.01	2.52	3.02	3.52	≥4.03
Macro section							Sticking
							

I = 200A, U = 20.0 cm/min

B

ø2.4mm wire							
DR(kg/h)	7.01	8.01	≥9.02				
Macro section			Sticking				
							
C-type filler							
DR(kg/h)	5.04	6.05	7.05	8.06	9.07	10.0	
Macro section							
DR(kg/h)	11.0	12.1	≥13.1				
Macro section			Sticking				
							

I = 500A, U = 60.0 cm/min

Fig. 5 – Macrosections according to the DR.

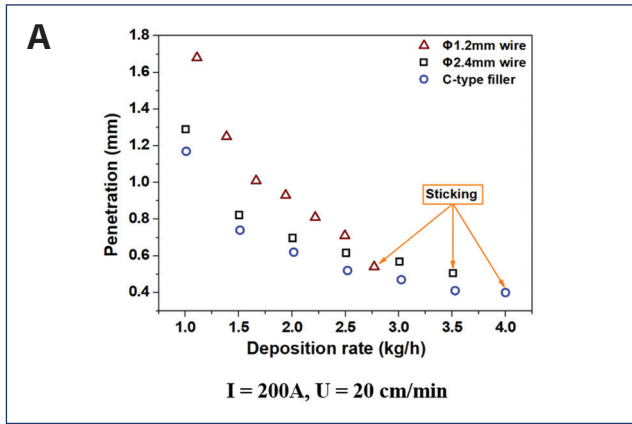


Fig. 6 – Relation between the DR and penetration depth.

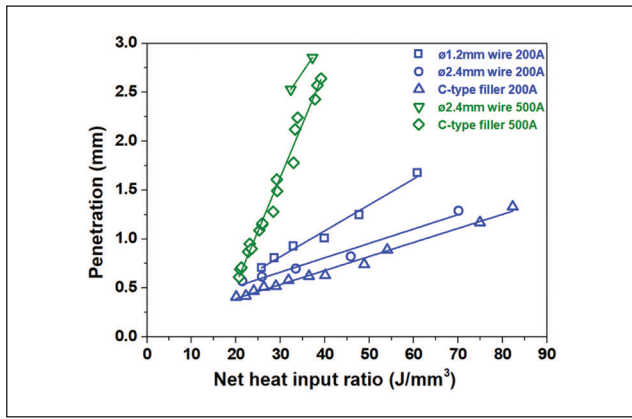
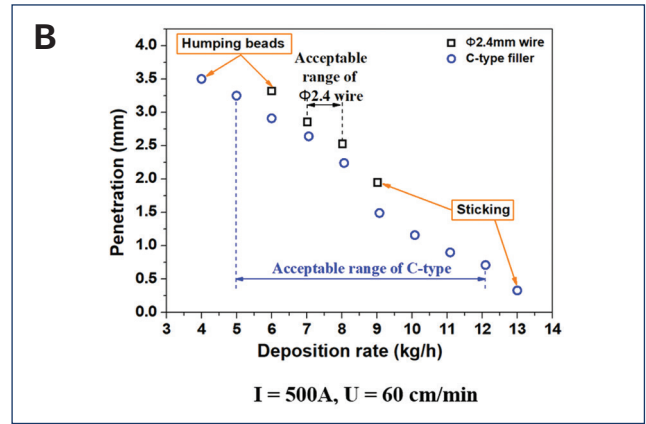


Fig. 7 – Relation between the NHIR and penetration depth of the $\phi 1.2$ -mm welding wire, $\phi 2.4$ -mm welding wire, and C-type filler metal at different welding currents.

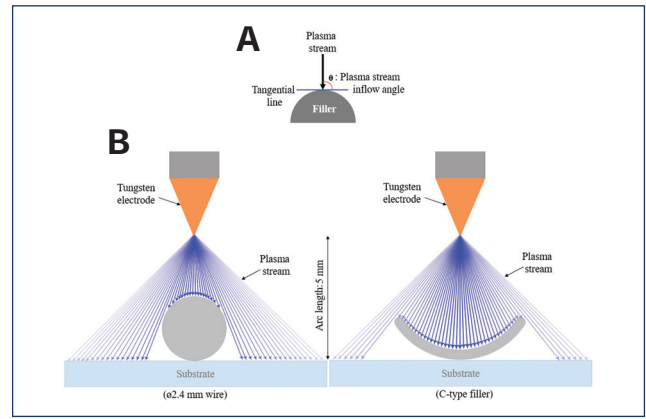


Fig. 8 – A – Definition of plasma stream inflow angle θ ; B – plasma stream inflow to the filler metal's top surface of the $\phi 2.4$ -mm welding wire and C-type filler metal.

Figure 6 shows the relationship between penetration depth and the DR for the $\phi 1.2$ -mm welding wire, $\phi 2.4$ -mm welding wire, and C-type filler metal at 200 and 500 A. In these two levels of welding currents, penetration depth decreased as the DR increased. Penetration depth by the C-type filler metal was lower than the $\phi 1.2$ - and $\phi 2.4$ -mm welding wires under the same welding current and DR. Additionally, penetration depth was not deep even though the welding current was high at 500 A for the C-type filler metal. The effect of filler metal feed speed on penetration depth was similar to the DR in that penetration depth decreased as the filler metal feed speed increased. This was because the DR was proportional to the filler metal feed speed for the same filler metal, as given in Equation 2. The acceptable range, which is shown in Fig. 6, was considered based on the sound welds without humping and sticking.

The maximum DR at a welding current of 200 A was 2.5 kg/h for a $\phi 1.2$ -mm welding wire, 3.0 kg/h (6.6 lb/h) for a $\phi 2.4$ -mm welding wire, and 3.5 kg/h for a C-type filler metal. At the same welding current of 200 A, the maximum DR of the C-type filler metal was 1.4 times that of the $\phi 1.2$ -mm welding wire and 1.17 times that of the $\phi 2.4$ -mm welding wire. At a welding current of 500 A, the $\phi 1.2$ -mm welding wire could not deposit the sound bead, and the acceptable DR range of

7–8 kg/h (15.3–17.6 lb/h) for the $\phi 2.4$ -mm welding wire was narrow. However, the acceptable DR range for the C-type filler metal was as broad as 5.04–12.1 kg/h. At 500 A, the maximum DR for the C-type filler metal was 1.51 times that of the $\phi 2.4$ -mm welding wire. For the same kind of filler metals, the maximum DR with 500 A was higher than with 200 A because the energy density of 500 A was higher than that of 200 A (Ref. 16). At the same current of 200 A, penetration depth was deepest in the $\phi 1.2$ -mm welding wire followed by the $\phi 2.4$ -mm welding wire. The C-type filler metal had the lowest penetration depth. At 500 A, the penetration depth of the C-type filler metal was lower than the $\phi 2.4$ -mm welding wire. Lower penetration depths are needed for some applications with high DRs, such as overlay welding and WAAM.

Figure 7 shows the relationship between the net heat input ratio (NHIR) and penetration depth for the $\phi 1.2$ - and $\phi 2.4$ -mm welding wires and the C-type filler metal. Penetration depth was linearly proportional to the NHIR for the $\phi 1.2$ -mm welding wire, $\phi 2.4$ -mm welding wire, and C-type filler metal. In the authors' previous research on C-type filler metals, penetration depth could be estimated using the NHIR during GTAW (Ref. 4). At the same NHIR, penetration depth was deepest for the $\phi 1.2$ -mm welding wire, medium for the $\phi 2.4$ -mm welding wire, and shallowest for the C-type filler metal at the same

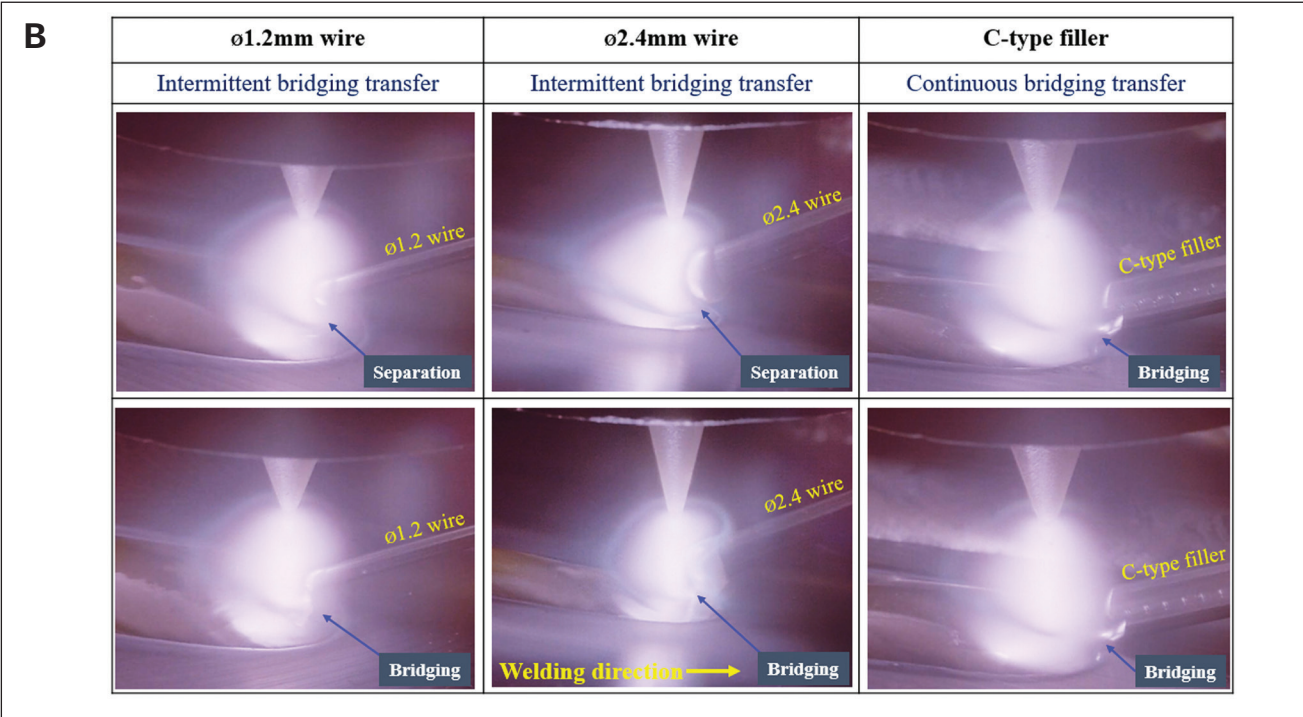
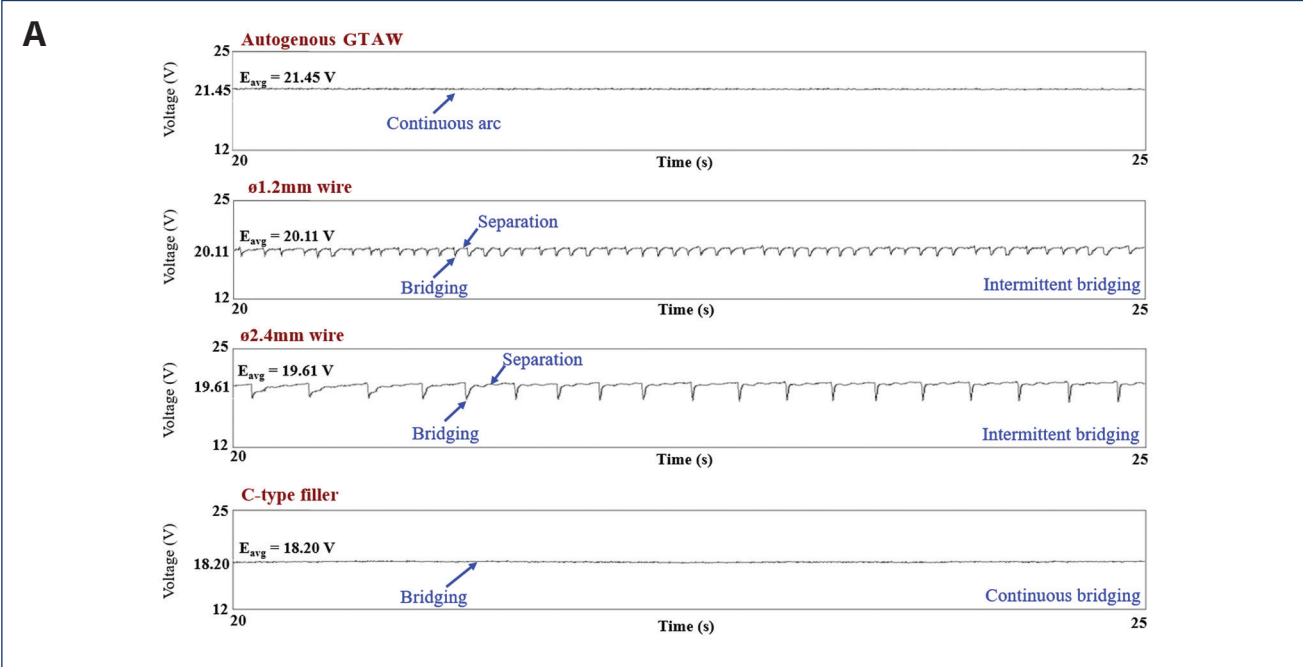


Fig. 9 – A – Comparison of metal transfer modes between the welding wires and C-type filler metal at a DR of 1 kg/h ($I = 200\text{ A}$, $U = 20\text{ cm/min}$); B – in-situ welding camera images of the filler metal's melting edge and molten bridge for the welding wires and C-type filler metal at a DR of 1 kg/h ($I = 200\text{ A}$, $U = 20\text{ cm/min}$).

welding current. Because of their varying cross-sectional areas, the filler metal feeding speeds for the three distinct filler metals/welding wires were not the same. At the same filler metal feed speed, the penetration depth of the $\phi 1.2\text{-mm}$ welding wire was deeper than the others. Additionally, the $\phi 2.4\text{-mm}$ welding wire was much deeper than the C-type filler metal. The filler metal feed speed or the DR effected

penetration depth at the same welding current and shape of the filler metal. The penetration depth estimation equation for each welding wire was developed by modifying the C-type filler metal's equation using a wide range of experimental data. Based on the aforementioned results, it can be said that penetration depth is governed by the NHIR, welding current, and shape of the filler metal.

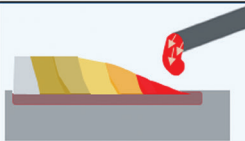
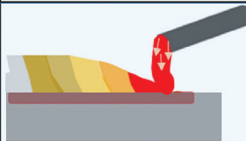
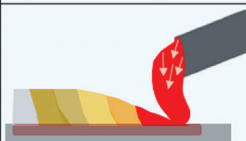
Filler type	Metal transfer	① Molten drop formation	② Molten drop growth	③ Bridging	④ Separation
Ø1.2mm wire	Intermittent bridging transfer				
		0.0 ms	0.045 ms	0.09 ms	0.1 ms
Ø2.4mm wire	Intermittent bridging transfer				
		0.0 ms	0.13 ms	0.026 ms	0.3 ms
C-type filler	Continuous bridging transfer				
		Bridging	Bridging	Bridging	Bridging

Fig. 10 – A dynamic series of metal transfers for the Ø1.2-mm welding wire, Ø2.4-mm welding wire, and C-type filler metal at a welding current of 200 A and a DR of 1 kg/h.

Effect of Plasma Stream Flow on the Welding Wire and C-Type Filler Metal

The current density of the plasma stream during GTAW can be considered as the Gaussian distribution (Ref. 16). The plasma stream inflow angle θ to filler metal surface was defined as the angle between the plasma stream and the tangential line of the surface — Fig. 8A. The plasma stream inflow efficiency was $\sin \theta$. The melting characteristics of the filler metals depended on the following: 1) the energy density of the plasma stream; 2) the inflow angle of the plasma stream; and 3) the filler metal surface area of the plasma stream inflow.

Figure 8B illustrates the plasma stream on the surface of the Ø2.4-mm welding wire and the C-type filler metal. The melting edges of both were positioned at the center of the electrode. The Ø2.4-mm welding wire was used because it has the same cross-sectional area as the C-type filler metal. The inflow angle θ from the center ($\theta = 90$ deg) to the edge ($\theta = 0$ deg) decreased rapidly for the welding wire, but for the C-type filler metal, the angle from the center ($\theta = 90$ deg) to the edge ($\theta = 70$ deg) decreased gradually. The plasma streamline inflow energy was the product of the plasma stream inflow efficiency $\sin \theta$ and the area of the filler metal surface. The arc length was defined as the distance between the bottom of the electrode tip and the surface of the substrate. The arc length distance was kept constant at 5 mm for both the welding wire and filler metal. The total inflow energy of the arc plasma on the C-type filler metal surface was higher than the welding wire. Therefore, the C-type filler metal's absorption of plasma inflow energy was higher than the circular welding wire's even though its cross-sectional area was the same. Therefore, the maximum DR of the C-type filler metal was higher than the wire at the same welding current.

Metal Transfer Characteristics in the Welding Wires and C-Type Filler Metal

Figures 9A and B show the arc voltage signals and in-situ images captured by the welding camera during metal transfer from the filler metal to the weld pool in the Ø1.2-mm welding wire, Ø2.4-mm welding wire, and C-type filler metal at a DR of 1 kg/h ($I = 200$ A, $U = 20$ cm/min [7.87 in./min]). The arc voltage for autogenous GTAW was used as a reference at an arc length of 5 mm. For the voltage waveforms of the Ø1.2- and Ø2.4-mm welding wires, the lower voltage meant bridging and the higher voltage meant separation. Intermittent bridging transfers occurred in the Ø1.2- and Ø2.4-mm welding wires, but continuous bridging transfer occurred in the C-type filler metal. The bridging sustainability of the welding wires was weak because the bridge was connected at the center point of the cross section in the welding wires. However, the bridging sustainability of the C-type filler metal was strong because the bridge was connected at the bottom point of the cross section in the C-type filler metal. The melting characteristics of the welding wires and C-type filler metal were intermittent, and the continuous bridging transfer modes are shown in Fig. 9B. The separation and bridging of the wires with the molten droplets are indicated in the images.

The dynamic series of metal transfer images for the Ø1.2-mm welding wire, Ø2.4-mm welding wire, and C-type filler metal are shown in Fig. 10. Even though these three welding wires/filler metals had the same welding current of 200 A and a DR of 1 kg/h, their metal transfer behaviors were different. Metal transfer occurrences in series were observed and depicted schematically. Even though the filler metal height before arc starting was 0 mm for all the welding wires/filler metals, separation happened due to the broken

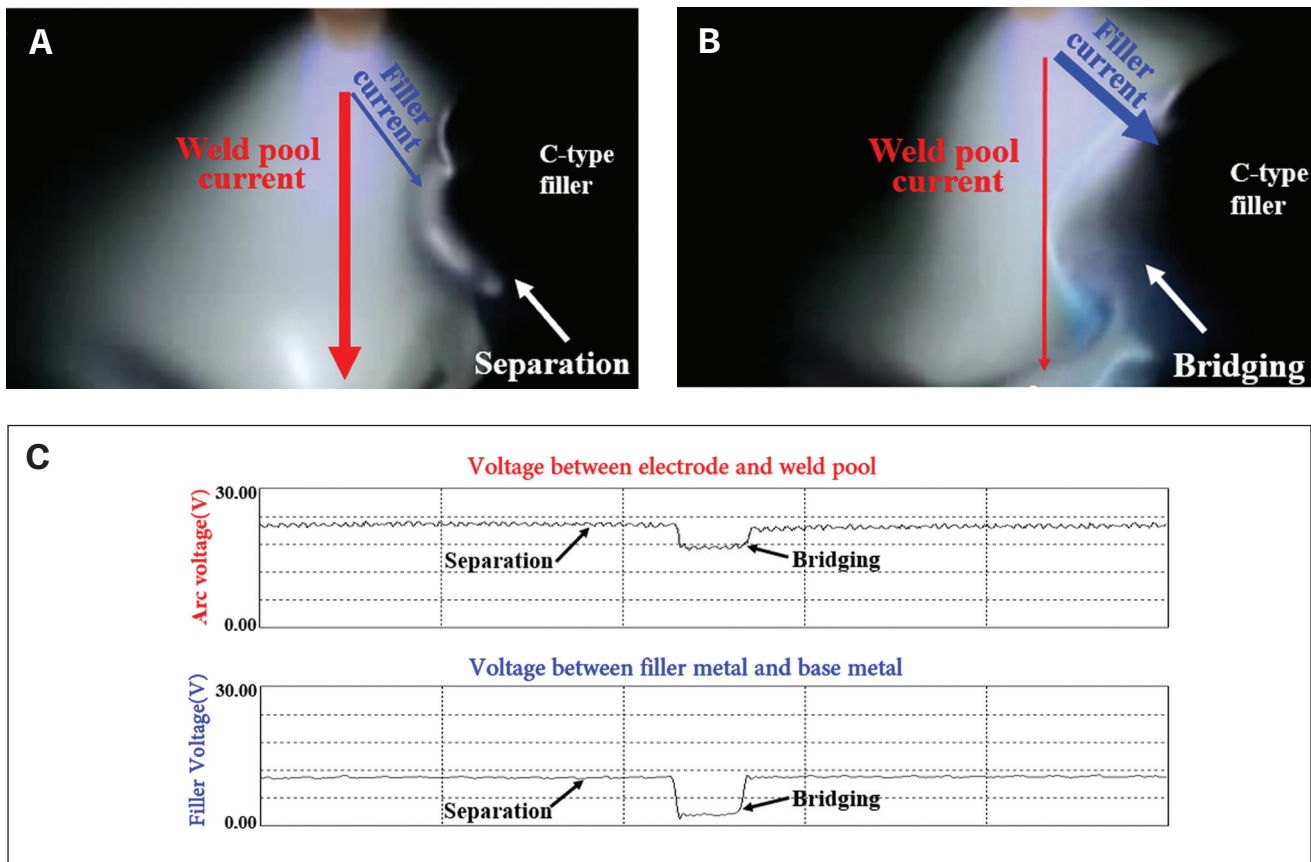


Fig. 11 — Change in weld pool current and filler metal current during the separation (A), bridging (B), and waveforms (C) of the arc voltage and filler metal voltage of the C-type filler metal.

bridge between the welding wire/filler metal and the weld pool because the bridging suitability was weak. On the other hand, the C-type filler metal showed continuous bridging transfer because the bridging sustainability was strong.

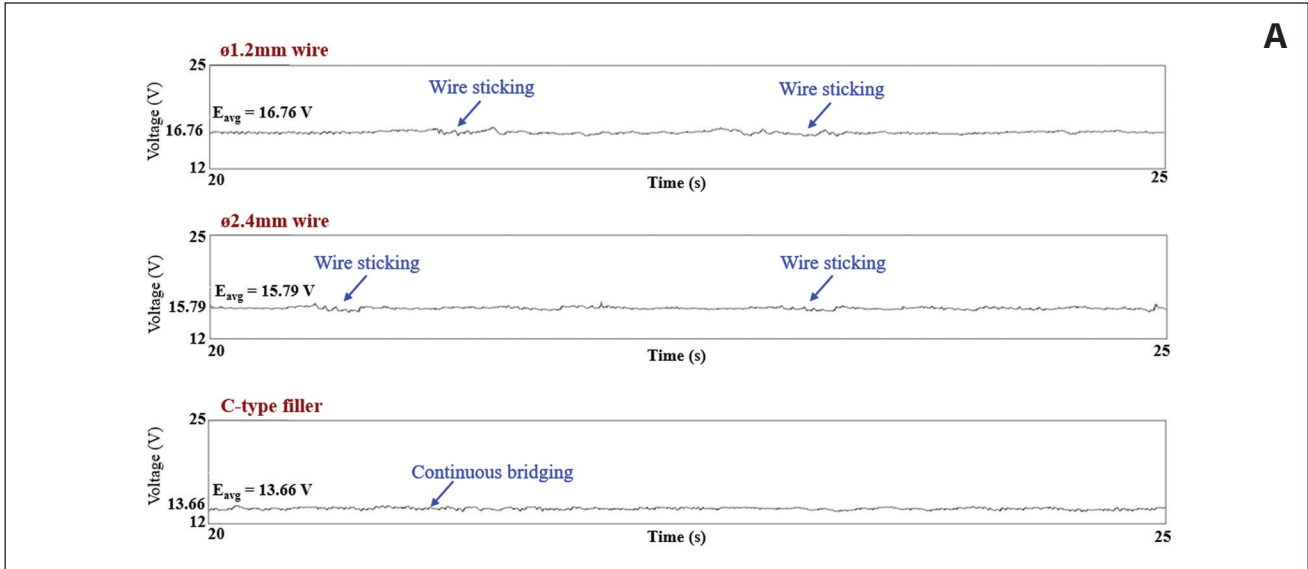
Figure 11 shows the change in weld pool current and filler metal current during the separation (Fig. 11A), bridging (Fig. 11B), and waveforms (Fig. 11C) of the arc voltage and filler metal voltage of the C-type filler metal (Ref. 5). The total arc current equaled the sum of the filler metal current and weld pool current. Based on what is shown in Fig. 11C, during separation, the filler voltage was higher than the bridging, so the filler metal resistance was higher than the bridging. Therefore, during bridging, the filler metal current could be high and the weld pool current could be low. While bridging transfer happened in the C-type filler metal, penetration depth was low and a humping bead could be prevented due to the low weld pool current — Fig. 11B. Additionally, the maximum DR of the C-type filler metal obtained was very high due to the high filler metal current.

Figures 12A and B show the arc voltage signals and in-situ images for a DR of 3.5 kg/h ($I = 200$ A, $U = 20$ cm/min). It was identified that welding wire sticking arose in the $\phi 1.2$ - and $\phi 2.4$ -mm circular welding wires, whereas continuous bridging arose in the C-type filler metal. Interrupted voltage signals were observed in the waveform for the welds made with both the $\phi 1.2$ - and $\phi 2.4$ -mm welding wires, indicating that the unmelted welding wire tip stuck to the weld bead and interfered with arc stability and bead formation. In contrast,

the C-type filler metal waveform was linear and stable with no voltage fluctuations at the same DR. Such a stable voltage waveform indicates a continuous bridging metal transfer for the C-type filler metal. As a result, the metal transfer characteristics of the welds made with the $\phi 1.2$ - and $\phi 2.4$ -mm welding wires differed from those of the C-type filler metal, resulting in the maximum DR for the C-type filler metal.

Figure 12B shows dynamic series images of the melting process in the welding wires and C-type filler metal at a DR of 3.5 kg/h. The dynamic series of images revealed sticking of the $\phi 1.2$ -mm welding wire with indications of an unmelted welding wire behind the electrode center, which progressively created a ring shape. During sticking, the bended wire was close to the electrode, which lowered the voltage potential. The welding wire melted quickly from the plasma stream then moved backward, which raised the voltage potential between the electrode tip and the weld pool, as shown by the voltage waveforms. Similarly, the $\phi 2.4$ -mm welding wire exhibited comparable sticking behavior, with the exception of the presence of the extended unmelted welding wire behind the electrode center. Examination of the dynamic series images, however, indicated that there was no difference in the continuous bridging transfer in the case of the C-type filler metal. As mentioned earlier, this was due to the high filler current and plasma stream inflow of the C-type filler metal advancing melting efficiency compared to the welding wires.

Figures 13A and B show the arc voltage signals and in-situ images for a DR of 5 kg/h, $I = 500$ A, $U = 60$ cm/min [23.6



Filler type (Metal transfer)	0.0 ms	20 ms	40 ms	60 ms
Ø1.2mm wire (Sticking)	Bead Wire			Unmelted wire
Ø2.4mm wire (Sticking)	Bead Wire			
C-type filler (Continuous bridging transfer)	Bead C-type filler			

Fig. 12 – A – Comparison of the metal transfer modes between the welding wires and C-type filler metal at a DR of 3.5 kg/h ($I = 200$ A, $U = 20$ cm/min); B – dynamic series images of the melting process in the welding wires and C-type filler metal at a DR of 3.5 kg/h ($I = 200$ A, $U = 20$ cm/min).

in./min]). For the autogenous GTAW, the waveform was characterized by significant voltage fluctuations. This was due to the high arc pressure, which caused deep and shallow depressions in the weld bead. Furthermore, deep and shallow depressions resulted in the generation of weld beads with humps and valleys. With waveform voltage fluctuations, a similar phenomenon was observed for the $\phi 1.2$ -mm welding wire. However, the voltage variation during deep and shallow depressions was smaller than during autogenous GTAW. Therefore, even though the $\phi 1.2$ -mm welding wire was fed into the arc column, the effect of arc pressure on the weld pool was still greater, causing humping beads. Consequently, the size or cross-sectional area of the $\phi 1.2$ -mm welding wire could not withstand the arc pressure and construct a strong metal transfer bridge between the filler metal and weld pool.

Hence, the melting edge of the wire was situated in front of the arc, increasing the distance between it and the weld pool.

When welding with the $\phi 2.4$ -mm welding wire, the intensity of the arc pressure was slightly reduced, and a minor number of deep and shallow depressions were generated. The waveform showed that the voltage fluctuated less for the $\phi 2.4$ -mm welding wire than for the $\phi 1.2$ -mm welding wire. When identifying the waveform of the C-type filler metal, the voltage signals were linear and stable with no variations. Therefore, the C-type filler metal can withstand a high arc pressure and maintain a continuous bridging transfer while also maintaining the link between the filler metal and the weld pool. As mentioned earlier, varying deep depressions caused by the $\phi 1.2$ -mm welding wire, $\phi 2.4$ -mm welding wire, and C-type filler metal are apparent in the still images — Fig. 13B. The weld pool depression size of

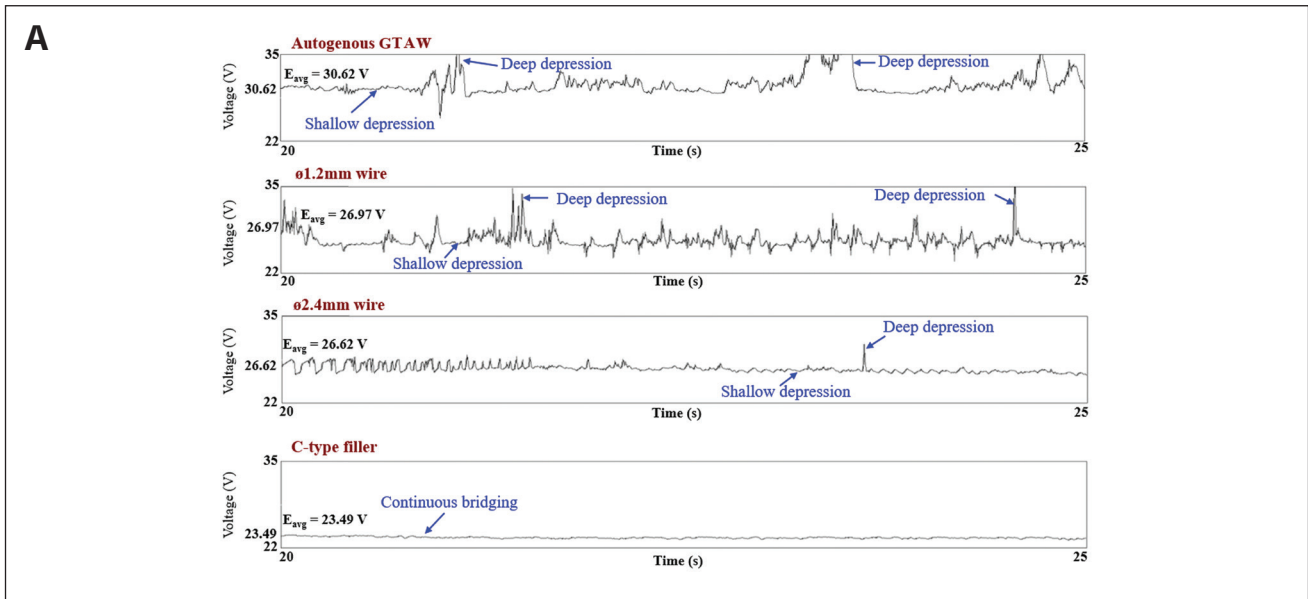


Fig. 13 – A – Comparison of metal transfer modes between the welding wires and C-type filler metal at a DR of 5 kg/h ($I = 500$ A, $U = 60$ cm/min); B – in-situ welding camera images of the filler metal’s melting edge and molten bridge for the welding wires and C-type filler metal at a DR of 5 kg/h ($I = 500$ A, $U = 60$ cm/min).

the ø1.2-mm welding wire was bigger than the ø2.4-mm welding wire followed by the C-type filler metal. The lower voltage occurred due to the shallow depression, and the higher voltage occurred due to the deep deformation. The shallow depression occurred through a bridging transfer. Deep depression occurred due to the separation of the bridge — Fig. 13A.

Figures 14A and B show the arc voltage signals and in-situ images for a DR of 9 kg/h ($I = 500$ A, $U = 60$ cm/min). Interrupted voltage signals were observed in the waveform for the welds made with the ø2.4-mm welding wire due to the wire sticking. In contrast, the waveform of the C-type filler metal was stable, indicating that a continuous bridging transfer occurred. The observations of in-situ images revealed sticking of the ø2.4-mm welding wire’s melting edge to the bead and minimal depression of the weld pool for the C-type filler metal — Fig. 14B.

Figure 15 shows the metal transfer characteristics of the welding wires and C-type filler metal at high and low DRs. At the high DR, the melting edge of the welding wires were behind the electrode center and the unmelted welding wires stuck to the bead surface. In contrast, the melting edge of

the C-type filler metal was located at the center of the electrode, where the plasma stream was stronger and enabled the C-type filler metal to melt efficiently at higher DRs. However, there was a difference in the metal transfer bridge connectivity in that the C-type filler metal had a thick bridge as well as a high bridge connectivity. Simultaneously, the wires had slender bridges, and their bridge connectivity was low.

However, when the DR was low, which meant the filler metal feeding speed was slow, the melting edge of the welding wires were away from the electrode center. The plasma stream melted the welding wires by generating a big drop, which detached from the welding wires’ tips and was transported to the weld pool when they became large enough. Because of the broken bridge with each droplet, the creation of a continuous metal transfer bridge was difficult for the welding wires and filler metal. At a lower DR, an elongated bridge was discovered for the C-type filler metal. Although both the welding wires and C-type filler metal deposited at the same rate (1 kg/h), the mode of metal transfer was different. The inflow energy of the plasma stream and the filler

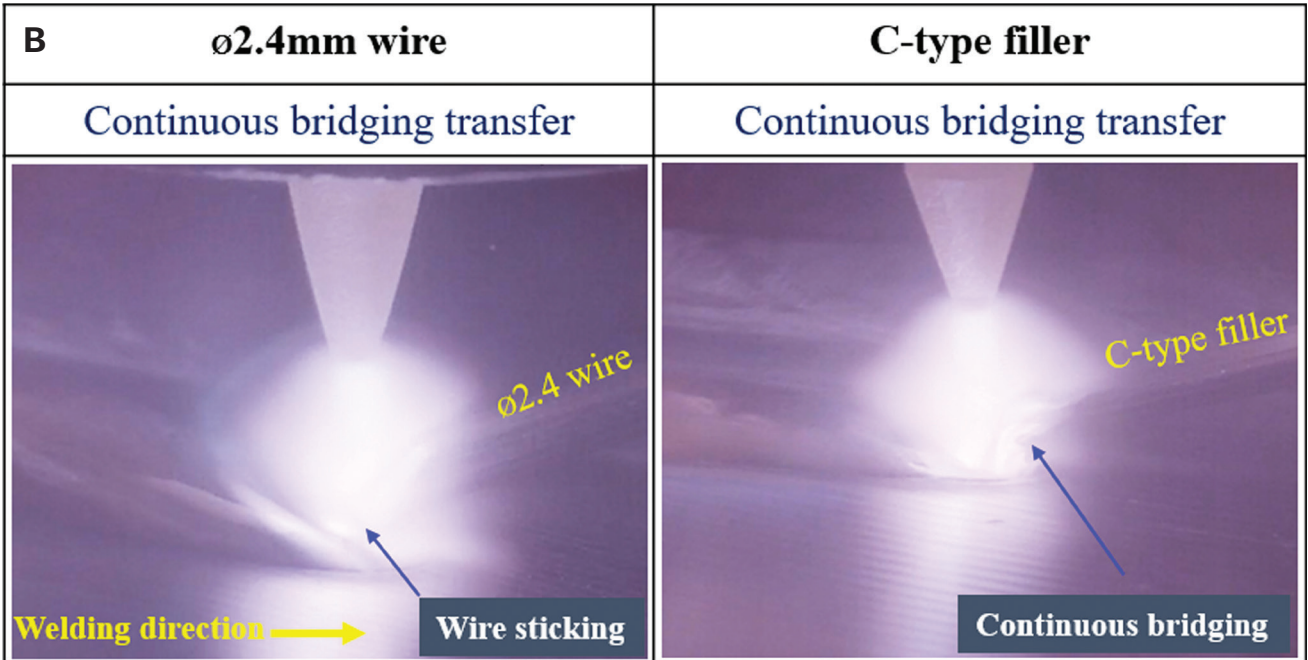
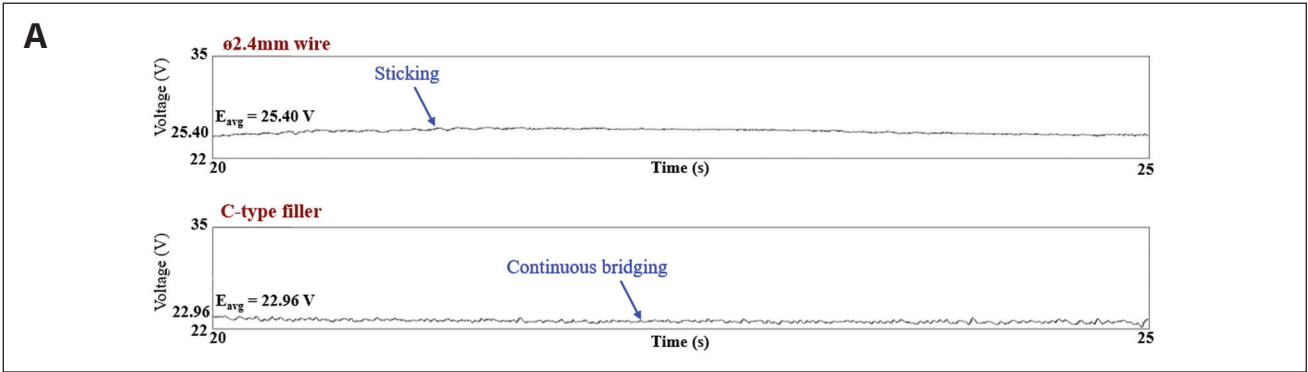


Fig. 14 – A – Comparison of metal transfer modes between the $\phi 2.4\text{-mm}$ welding wire and C-type filler metal at a DR of 9 kg/h ($I = 500\text{ A}$, $U = 60\text{ cm/min}$); B – in-situ welding camera images of the filler metal's melting edge and molten bridge for the welding wires and C-type filler metal at a DR of 9 kg/h ($I = 500\text{ A}$, $U = 60\text{ cm/min}$).

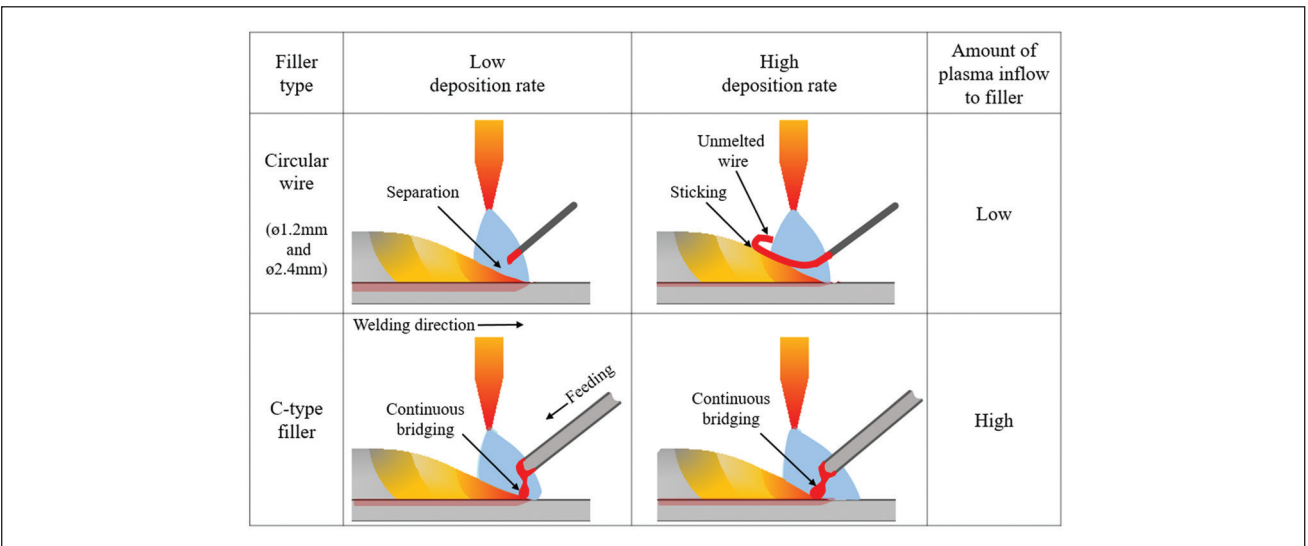


Fig. 15 – Schematic diagram of the metal transfer mode in the circular welding wires and C-type filler metal.

metal current were greater in the C-type filler metal than in the welding wires. Consequently, the welding wires received an intermittent bridging transfer while the C-type filler metal obtained a continuous bridging transfer. Also, at the high-current region, continuous bridging transfer was sustained in the C-type filler metal. Therefore, in the high-current region of 500 A, where the DR was low at 5 kg/h, sound beads of shallow depression were obtained. However, humping beads appeared in the welding wires due to the deep depression caused by the separation of the bridge.

Conclusions

This study investigated the maximum DR and melting characteristics using a ϕ 1.2-mm welding wire (1.1 mm²), ϕ 2.4-mm welding wire (4.5 mm²), and C-type filler metal (5.0 mm²) of Alloy 625 during GTAW. The welding method involved bead-on-plate welds in a flat position using an industrial robot. The conclusions of this study are as follows:

1) At the same welding current of 200 A, the maximum DR of the C-type filler metal was 1.4 times that of the ϕ 1.2-mm welding wire and 1.17 times that of the ϕ 2.4-mm welding wire. At a welding current of 500 A, it was impossible for the ϕ 1.2-mm welding wire to deposit sound beads, and the acceptable DR range for the ϕ 2.4-mm welding wire was narrow (i.e., 7–8 kg/h). However, the acceptable DR range for the C-type filler metal was as broad as 5.04–12.1 kg/h. The maximum DR for the C-type filler metal was 1.51 times that of the ϕ 2.4-mm welding wire.

2) The melting characteristics of the filler metals depended on the following: 1) the energy density of the plasma stream; 2) the inflow angle of the plasma stream; and 3) the filler metal surface area of the plasma stream inflow. The plasma inflow angle in the welding wires rapidly decreased from 90 to 0 deg as the arc angle increased from the top center point to both sides. However, in the C-type filler metal, the plasma inflow angle decreased slightly as the arc angle increased from the bottom center point to both sides. Therefore, the amount of plasma inflow to the C-type filler metal was much higher than that to the welding wires. As a result, the maximum DR was high for the same welding current.

3) At the same current of 200 A, the penetration depth was deepest in the ϕ 1.2-mm welding wire followed by the ϕ 2.4-mm welding wire, and the C-type filler metal had the lowest penetration depth. At 500 A, the penetration depth of the C-type filler metal was lower than the ϕ 2.4-mm welding wire. This was because the filler metal current of the C-type filler metal was higher than the ϕ 1.2- and ϕ 2.4-mm welding wires. Also, the weld pool current of the C-type filler metal was lower than the ϕ 1.2 and ϕ 2.4-mm welding wires.

4) In the high-current region of 500 A, where the DR was low at 5 kg/h, sound beads of shallow depression were obtained in the C-type filler metal owing to the continuous bridging transfer. However, humping beads appeared in the wires due to the deep depression caused by the separation of the bridge.

Acknowledgments

This research was supported by the Korea Evaluation Institute of Industrial Technology (KEIT), Daegu, South Korea,

under the Ministry of Trade, Industry and Energy (MOTIE), South Korea, Grant No. 20004932.

References

1. Chen, J. S., Lu, Y., Li, X. R., and Zhang, Y. M. 2012. Gas tungsten arc welding using an arcing wire. *Welding Journal* 91(10): 261-s to 269-s.
2. Meng, X., Qin, G., Bai, X., and Zou, Z. 2016. Humping phenomena in high-speed GTAW of different weld penetrations. *Welding Journal* 95(9): 331-s to 339-s.
3. Cho, S.-M., Oh, D.-S., Ham, H.-S., Ha, H.-J., Shin, H.-S., Jun, J.-H., Byun, J.-G., Park, J.-H., and Kwon, H.-Y. 2016. Filler metal for TIG welding. U.S. Patent US20160199947A1.
4. Cheepu, M., Baek, H. J., Kim, Y. S., and Cho, S. M. 2022. Penetration estimation of GTAW with C-Type filler by net heat input ratio. *Welding Journal* 101(9): 240-s to 248-s. DOI: 10.29391/2022.101.018
5. Jun, J. H., Park, J. H., Cheepu, M., and Cho, S. M. 2020. Observation and analysis of metal transfer phenomena for high-current super-TIG welding process. *Science and Technology of Welding and Joining* 25(2): 106–111. DOI: 10.1080/13621718.2019.1637172
6. Jun, J.-H., Kim, S.-R., and Cho, S.-M. 2016. A study on productivity improvement in narrow gap TIG welding. *Journal of Welding and Joining* 34(1): 68–74. DOI: 10.5781/JWJ.2016.34.1.68
7. Park, J.-H., Kim, Y.-H., Baek, H.-J., and Cho, S.-M. 2019. A study on process development of super-TIG welding for 9% nickel steel with Alloy 625. *Journal of Manufacturing Process* 40: 140–148. DOI: 10.1016/j.jmapro.2019.03.017
8. Cheepu, M., Lee, C. I., and Cho, S. M. 2020. Microstructural characteristics of wire arc additive manufacturing with Inconel 625 by super-TIG welding. *Transactions of the Indian Institute of Metals* 73(6): 1475–1479. DOI: 10.1007/s12666-020-01915-x
9. Park, J. H., Park, S. Y., and Cho, S. M. 2019. A study on process development of deformation reduction in TIG overlay welding. *Journal of Welding and Joining* 37(1): 82–88. DOI: 10.5781/JWJ.2019.37.1.11
10. Yudodibroto, B. Y. B., Hermans, M. J. M., Hirata, Y., and den Ouden, G. 2004. Influence of filler wire addition on weld pool oscillation during gas tungsten arc welding. *Science and Technology of Welding and Joining* 9(2): 163–168. DOI: 10.1179/136217104225012274
11. ISO/TR 18491, *Welding and allied processes — Guidelines for measurement of welding energies*. 2015. Geneva, Switzerland: International Organization for Standardization.
12. DuPont, J. N., and Marder, A. R. 1995. Thermal efficiency of arc welding processes. *Welding Journal* 74(12): 406-s to 416-s.
13. Jenney, C. L., and O'Brien, A., eds. 2001. "Chapter 10 — Monitoring and Control of Welding and Joining Processes." In *Welding Handbook, Welding Science and Technology*, Vol. 1, 9th Ed. Miami, Fla.: American Welding Society.
14. DuPont, J. N., and Marder, A. R. 1996. Dilution in single pass arc welds. *Metallurgical and Materials Transactions B* 27(3): 481–489.
15. Shirali, A. A., and Mills, K. C. 1993. The effect of welding parameters on penetration in GTA welds. *Welding Journal* 72(7): 347-s to 353-s.
16. Oh, D.-S., Kim, Y.-S., and Cho, S.-M. 2005. Derivation of current density distribution by arc pressure measurement in GTA welding. *Science and Technology of Welding and Joining* 10(4): 442–446. DOI: 10.1179/174329305X44116

MURALIMOHAN CHEEPU (muralicheepu@gmail.com), **HYO JIN BAEK**, **YOUNG SIK KIM**, and **SANG MYUNG CHO** are with STARWELDS Inc., Busan, Republic of Korea.